Proceedings of the 16th International IEEE Annual Conference on
Intelligent Transportation Systems (ITSC 2013), The Hague, The
Netherlands, October 6-9, 2013

MoC4.4

Linear Model Predictive Control for
Lane Keeping and Obstacle Avoidance on Low Curvature Roads

Valerio Turri*, Ashwin Carvalho†, Hongtei Eric Tseng♯, Karl Henrik Johansson*, Francesco Borrelli†

Abstract— This paper presents a control architecture based
on a linear MPC formulation that addresses the lane keeping
and obstacle avoidance problems for a passenger car driving
on low curvature roads. The proposed control design decouples
the longitudinal and lateral dynamics in two successive stages.
First, plausible braking or throttle profiles are defined over the
prediction horizon. Then, based on these profiles, linear time-
varying models of the vehicle lateral dynamics are derived and
used to formulate the associated linear MPC problems. The
solutions of the optimization problems are used to determine for
every time step, the optimal braking or throttle command and
the corresponding steering angle command. Simulations show
the ability of the controller to overcome multiple obstacles and
keep the lane. Experimental results on an autonomous passen-
ger vehicle driving on slippery roads show the effectiveness of
the approach.

I. INTRODUCTION

Over the last two decades, the increased presence of elec-
tronics and software in vehicles has allowed the introduction
of several active safety systems, e.g., Anti-lock Braking
System (ABS), Electronic Stability Control (ESC), Adaptive
Cruise Control (ACC). Nevertheless, the number of fatal
road traffic incidents due to driver distraction and speeding
is still significantly high [1]. Recent advances in sensing
technologies and 3D environment reconstruction [2]–[4] have
opened up new possibilities and have provided a base for
the design of advanced autonomous and semi-autonomous
guidance systems.

Because of its capability of systematically handling non-
linear time-varying models and constraints, and operating
close to the limits of admissible states and inputs, Model
Predictive Control (MPC) has been widely used to address
the autonomous vehicle guidance problem [5]–[10]. In [5],
the MPC problem has been formulated as a quadratic pro-
gram (QP) by limiting the intervention to the steering, and
linearizing the vehicle dynamics around a constant vehicle
speed and small slip angles. In [8]–[10], the authors address
the problem of integrated braking and steering control by
using a hierarchical control architecture. A high-level con-
troller generates an obstacle-free trajectory, while a low level
controller tracks this planned trajectory. In order to combine
braking and steering, both levels implement a nonlinear
MPC formulation which requires the online solution of a
non-convex optimization problem. In order to reduce the
real-time computational complexity, in [9], the authors have
proposed the use of a spatial vehicle model which simplifies
the problem. However, the nonlinear nature of the model
used in the MPC problem significantly limits the maximum
prediction horizon implementable.

In this paper, we propose a linear MPC-based control
architecture suitable for vehicles driving in low curvature

* ACCESS Linnaeus Center and School of Electric Engineering, Royal
Institute of Technology, Stockholm, Sweden
† Department of Mechanical Engineering, University of California,
Berkeley, USA
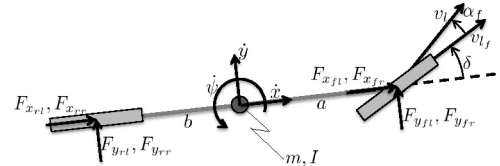♯ Powertrain Control R&A, Ford Motor Company, Dearborn, MI, U.S.A.

Fig. 1.   Illustration for the bicycle model.

roads, such as highways. It addresses the lane-keeping and
obstacle avoidance problems by combining steering and
braking actions. In particular, the paper presents two main
contributions: first, under the assumption of a large radius of
curvature, we derive a linear time-varying (LTV) model of
the vehicle lateral dynamics, as a function of the longitudinal
braking or throttle profile; second, we use this model to for-
mulate a linear MPC problem for lane-keeping and obstacle
avoidance, accounting for both the longitudinal and lateral
dynamics. The linearity of the model allows us to recast the
MPC problem as a set of convex QPs and, hence, to reduce
the overall computational complexity of the problem.

The rest of the paper is organized as follows: in Section
II, we introduce the *extended* bicycle model and show how it
can be simplified to obtain a LTV model of the vehicle lateral
dynamics. In Section III, we show how the objectives of lane
keeping and obstacle avoidance are formulated as convex
constraints on the vehicle's states and inputs. In Section
IV, we introduce the linear MPC formulation. In Section V,
we demonstrate the effectiveness of the proposed controller
through hardware-in-the-loop simulations and experiments
on a real passenger vehicle. Finally, in Section VI, we
provide some concluding remarks and outline future work.

II. VEHICLE MODEL

In this section, we present a modified version of the vehi-
cle bicycle model [6] and the corresponding simplified LTV
model of the lateral dynamics used in the MPC formulation.

A. The extended bicycle model

In this paper we are using a modified version of the clas-
sical bicycle model, that also accounts for the longitudinal
and lateral load transfers while computing the forces acting
on the tires. Therefore, the *extended* bicycle model can be
considered as a trade-off between the classical bicycle model
and the four wheel vehicle model [11].

Bicycle model equations

The notation used in the vehicle model is shown in
Figure 1. The vehicle dynamics are described by the fol-
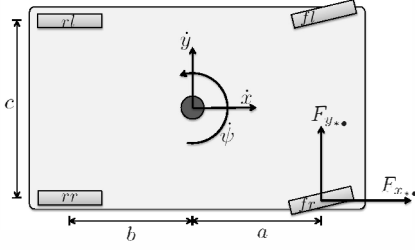
Fig. 2. Sketch of the vehicle and modeling notation for the computation of the longitudinal and lateral load transfers.
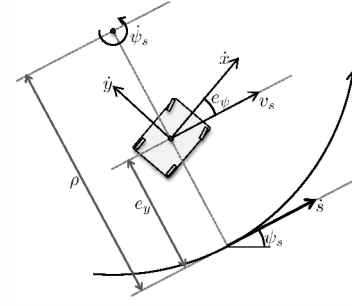

Fig. 3. The curvilinear coordinate system. The dynamics are derived about a curve defining the centerline of a track. The coordinate s defines the arc-length along the track.

lowing set of differential equations:

$$m\ddot{x} = F_{x_{fl}} + F_{x_{fr}} + F_{x_{rl}} + F_{x_{rr}} - k_d\dot{x}^2 \quad \text{(1a)}$$

$$m\ddot{y} = -m\dot{x}\dot{\psi} + F_{y_{fl}} + F_{y_{fr}} + F_{y_{rl}} + F_{y_{rr}} \quad \text{(1b)}$$

$$I\ddot{\psi} = a(F_{y_{fl}} + F_{y_{fr}}) - b(F_{y_{rl}} + F_{y_{rr}}), \quad \text{(1c)}$$

where $\dot{x}$ and $\dot{y}$ denote the longitudinal and the lateral speed of the vehicle, and $\dot{\psi}$ denotes the yaw rate. The constants m and I denote the vehicle's mass and rotational inertia about the yaw axis, respectively, and a and b denote the distances from the center of gravity (CoG) to the front and rear axles, respectively. In Equation (1a), $-k_d\dot{x}^2$ represents the aerodynamic longitudinal force with $k_d = \frac{1}{2}\rho C_d S_d$, where ρ is the air density, C_d is the aerodynamic drag coefficient and S_d is the vehicle frontal cross section. $F_{x_{*\bullet}}$ and $F_{y_{*\bullet}}$ (where $* = f, r, \bullet = l, r$) are the tire forces acting along the vehicle longitudinal and lateral axes relative to each wheel. These forces are related to the forces $f_{x_{*\bullet}}$ and $f_{y_{*\bullet}}$ acting along the wheel longitudinal and lateral axes, respectively, through an equality for the rear wheels ($F_{x_{r\bullet}} = f_{x_{r\bullet}}$, $F_{y_{r\bullet}} = f_{y_{r\bullet}}$) and a rotation depending on the steering angle δ for the front wheels ($F_{x_{f\bullet}} = f_{x_{f\bullet}}\cos(\delta) - f_{y_{f\bullet}}\sin(\delta)$, $F_{y_{f\bullet}} = f_{x_{f\bullet}}\sin(\delta) + f_{y_{f\bullet}}\cos(\delta)$).

Tire forces

In connection to the computation of the longitudinal and lateral load transfers, we introduce the following assumption.

Assumption 1: In the load transfer computation, the effect of the aerodynamic forces acting on the vehicle is negligible. Considering the sketch in Figure 2, we can derive the forces acting along the vehicle vertical axis of each wheel $F_{z_{*\bullet}}$ due to the load transfer as,

$$F_{z_{fl}} = \frac{bF_z - eF_x}{2(a+b)} - \frac{eF_y}{2c}, \quad F_{z_{fr}} = \frac{bF_z - eF_x}{2(a+b)} + \frac{eF_y}{2c},$$
$$F_{z_{rl}} = \frac{aF_z + eF_x}{2(a+b)} - \frac{eF_y}{2c}, \quad F_{z_{rr}} = \frac{aF_z + eF_x}{2(a+b)} + \frac{eF_y}{2c}. \quad \text{(2)}$$

where $F_x = \sum_{*=f,r;\bullet=l,r} F_{x_{*\bullet}}$, $F_y = \sum_{*=f,r;\bullet=l,r} F_{y_{*\bullet}}$ and $F_z = mg$ are the cumulative forces acting on the wheels along the longitudinal, lateral and vertical vehicle axes, respectively; the constants c and e denote respectively the vehicle width and the height of the CoG and g is the gravitational acceleration.

The second input of the model is the braking ratio, denoted as β, with $\beta = -1$ corresponding to maximum braking and $\beta = 1$ corresponding to maximum throttle. We introduce the following assumptions regarding the longitudinal forces:

Assumption 2: The rotational inertia of the wheels is negligible. The torque $T_{x_{*\bullet}}$ about the wheel's axis produces

a longitudinal force $f_{x_{*\bullet}} = T_{x_{*\bullet}}/r$, where r is the wheel's radius.

Assumption 3: The low level controller of the longitudinal dynamics distributes the forces as

$$f_{x_{*\bullet}} = F_{z_{*\bullet}}\mu\beta, \quad \text{(3)}$$

where μ denotes the friction coefficient between the tire and the road surface.

Note that $F_{z_{*\bullet}}$ and, consequently $f_{x_{*\bullet}}$, depend on F_x and F_y. The force component $f_{y_{*\bullet}}$ can be computed using a simplified version of the semi-empirical Pacejka formula [12] as $f_{y_{*\bullet}} = \sqrt{(\mu F_{z_{*\bullet}})^2 - f_{x_{*\bullet}}^2}\sin(C\arctan(B\alpha_*))$, where C and B are tire parameters calibrated using experimental data. The variable α_* denotes the slip angles of the front and rear wheels, which can be computed as,

$$\alpha_f = \frac{\dot{y} + a\dot{\psi}}{\dot{x}} - \delta, \quad \alpha_r = \frac{\dot{y} - b\dot{\psi}}{\dot{x}}. \quad \text{(4)}$$

Substituting (3) in the expression of $f_{y_{*\bullet}}$, we obtain an alternate representation of the lateral forces which emphasizes the linear relationship between $f_{y_{*\bullet}}$ and $F_{z_{*\bullet}}$

$$f_{y_{*\bullet}} = \mu F_{z_{*\bullet}}\sqrt{1 - \beta^2}\sin(C\arctan(B\alpha_*)). \quad \text{(5)}$$

As we will show in the subsection II-B, this linear relationship allows us to decouple the longitudinal dynamics from the lateral dynamics.

Road curvilinear coordinate system

Figure 3 shows the curvilinear coordinate system describing the interaction between the vehicle and the road, which can be used to derive the following kinematic equations:

$$\dot{e}_\psi = \dot{\psi} - \dot{\psi}_s$$
$$\dot{e}_y = \dot{y}\cos(e_\psi) + \dot{x}\sin(e_\psi)$$
$$\dot{s} = \frac{\rho}{\rho - e_y}(\dot{x}\cos(e_\psi) - \dot{y}\sin(e_\psi)), \quad \text{(6)}$$

where e_ψ and e_y denote the heading angle error and the lateral position error relative to the road centerline, respectively, and s denotes the projected vehicle position along the road centerline. ρ and ψ_s are the radius of the curvature and the heading of the road centerline, respectively. $\dot{\psi}_s$ is the time derivative of ψ_s and depends on $\dot{s}$ according to the relation $\dot{\psi}_s = \dot{s}/\rho$. We also define $\psi_r = \frac{d\psi_s}{ds}$ as the derivative of ψ_s with respect to the curvilinear coordinate s. ψ_r is the inverse of ρ and is assumed to be known.

The differential equations (1)–(6) completely define the extended bicycle model.

B. A LTV model for the vehicle lateral dynamics

In this subsection we present the simplifications required to obtain a LTV model of the lateral dynamics from the extended bicycle model. The discretized version of this model will be used in section IV to formulate the MPC problem.

The following assumptions are introduced.

Assumption 4: The braking ratio $\beta(t)$ is assumed to be constant over the prediction horizon (i.e., $\beta(t) = \bar{\beta}$).

Assumption 5: The vehicle is driven in a typical highway scenario (i.e. high speed limit and low curvature lane), which implies that:

- the heading angle error is small (i.e., $e_\psi \simeq 0$),
- the steering angle necessary to reach the tire saturation is small (i.e., $\delta \simeq 0$).

Assumption 5 also implies: $\cos(\delta) \simeq 1$, $\sin(\delta) \simeq \delta \simeq 0$, $\cos(e_\psi) \simeq 1$, $\sin(e_\psi) \simeq e_\psi$, $\frac{\rho}{\rho - e_y} \simeq 1$.

In summary we can rewrite the vehicle model as:

$$m\ddot{x} = mg\mu\bar{\beta} - k_d \dot{x}^2 \tag{7a}$$

$$m\ddot{y} = -m\dot{x}\dot{\psi} + F_{y_f} + F_{y_r} \tag{7b}$$

$$I\ddot{\psi} = aF_{y_f} - bF_{y_r} \tag{7c}$$

$$\dot{e}_\psi = \dot{\psi} - \dot{x}\psi_r \tag{7d}$$

$$\dot{e}_y = \dot{y} + \dot{x}e_\psi \tag{7e}$$

$$\dot{s} = \dot{x}, \tag{7f}$$

where $F_{y_*} = F_{y_{*l}} + F_{y_{*r}}$. Additionally $F_{x_{*\bullet}} = f_{x_{*\bullet}}$ and $F_{y_{*\bullet}} = f_{y_{*\bullet}}$, where $* = f, r$; $\bullet = r, l$. Note that (7a) and (7f) completely define the longitudinal dynamics of the vehicle. Therefore, given the input β, the initial speed $\dot{x}(t_0)$ and position $s(t_0)$ of the vehicle, the differential equations (7a) and (7f) can be integrated to obtain explicit expressions of the speed $\bar{\dot{x}}(t)$ and position $\bar{s}(t)$, respectively.

The only nonlinearity in the remaining differential equations (7b)–(7e) is contained in the terms $F_{y_f}(\alpha_f)$ and $F_{y_r}(\alpha_r)$, whose expressions can be rewritten by combining (2), (4) and (5) as

$$F_{y_f} = \mu \frac{(b - e\bar{\beta})mg}{a + b}\sqrt{1 - \bar{\beta}^2}\sin(C\arctan(B\alpha_f)),$$

$$F_{y_r} = \mu \frac{(a + e\bar{\beta})mg}{a + b}\sqrt{1 - \bar{\beta}^2}\sin(C\arctan(B\alpha_r)). \tag{8}$$

Figure 4 displays $F_{y_*}(\alpha_*)$ for a given value of $\bar{\beta}$ and shows how F_{y_*} can be bounded by two linear functions,

$$C_{*_L}\alpha_* \leq F_{y_*} \leq C_{*_U}\alpha_*,$$

where C_{*_U} and C_{*_L} are functions of the parameters in (8). The corresponding slip angle intervals in which the upper and lower approximations are valid are denoted as $[-\alpha_{*,lim_U}, \alpha_{*,lim_U}]$ and $[-\alpha_{*,lim_L}, \alpha_{*,lim_L}]$, respectively. f_{toll} denotes the maximum acceptable error in the linear approximations of the tire lateral forces.

These approximations allow us to define the following two LTV models of the lateral vehicle dynamics:

- *Conservative lateral dynamics model:* This model underestimates the cornering ability of the vehicle. In particular, F_{y_f} and F_{y_r} in (7b) are approximated by $C_{f_L}(\bar{\beta})\alpha_f$ and $C_{r_L}(\bar{\beta})\alpha_r$, respectively, and F_{y_f} and F_{y_r} in (7c) are approximated by $C_{f_L}(\bar{\beta})\alpha_f$ and
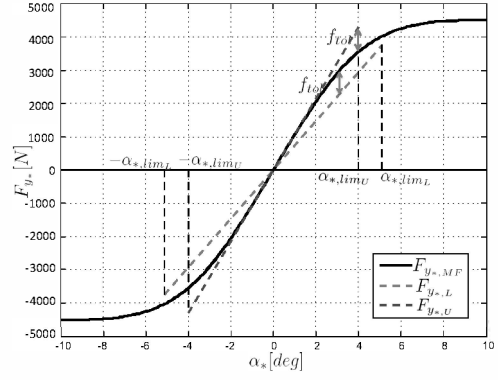

Fig. 4. Plots of the lateral force computed with the simplified Magic Formula ($F_{y_*,MF}$), with the lower ($F_{y_*,L}$) and the upper ($F_{y_*,U}$) linear approximation, for a given value of the vertical force and longitudinal force.

$C_{r_U}(\bar{\beta})\alpha_r$. Therefore, the resulting conservative lateral dynamics model can be expressed as:

$$m\ddot{y} = -m\dot{x}\dot{\psi} + C_{f_L}\alpha_f + C_{r_L}\alpha_r$$

$$I\ddot{\psi} = aC_{f_L}\alpha_f - bC_{r_U}\alpha_r$$

$$\dot{e}_\psi = \dot{\psi} - \dot{x}\psi_r \tag{9}$$

$$\dot{e}_y = \dot{y} + \bar{\dot{x}}e_\psi$$

$$\dot{\delta} = u,$$

where $\alpha_f = (\frac{\dot{y} + a\dot{\psi}}{\bar{\dot{x}}} - \delta)$ and $\alpha_r = \frac{\dot{y} - b\dot{\psi}}{\bar{\dot{x}}}$. The term "*conservative*" emphasizes the robustness of the model to the nonlinear tire characteristics. This model plays the main role in the MPC formulation.

Note that the steering angle δ has been added to the state space, while the new input variable is the steering rate, denoted by u. This modification allows us to keep the inputs constant over certain time intervals while continuously varying the steering angle. A similar modification has been introduced in the next model.

- *Overreacting lateral dynamics model:* This model overestimates the cornering ability of the vehicle. In particular, F_{y_f} and F_{y_r} in (7b) are approximated by $C_{f_U}(\bar{\beta})\alpha_f$ and $C_{r_U}(\bar{\beta})\alpha_r$, respectively, and F_{y_f} and F_{y_r} in (7c) are approximated by $C_{f_U}(\bar{\beta})\alpha_f$ and $C_{r_L}(\bar{\beta})\alpha_r$, respectively. The resulting overreacting lateral dynamics model can be written as,

$$m\ddot{y} = -m\dot{x}\dot{\psi} + C_{f_U}\alpha_f + C_{r_U}\alpha_r$$

$$I\ddot{\psi} = aC_{f_U}\alpha_f - bC_{r_L}\alpha_r$$

$$\dot{e}_\psi = \dot{\psi} - \dot{x}\psi_r \tag{10}$$

$$\dot{e}_y = \dot{y} + \bar{\dot{x}}e_\psi$$

$$\dot{\delta} = u,$$

where $\alpha_f = \frac{\dot{y} + a\dot{\psi}}{\bar{\dot{x}}} - \delta$ and $\alpha_r = \frac{\dot{y} - b\dot{\psi}}{\bar{\dot{x}}}$.

Both models hold for slip angles α_f and α_r inside the intervals

$$|\alpha_f| \leq \alpha_{f,lim}, \qquad |\alpha_r| \leq \alpha_{r,lim}, \tag{11}$$

where $\alpha_{f,lim} = \min\{\alpha_{f,lim_U}, \alpha_{f,lim_L}\}$ and $\alpha_{r,lim} = \min\{\alpha_{r,lim_U}, \alpha_{r,lim_L}\}$. Even if the slip angles doesn't have the same sign over the horizon, through simulations it

has been possible to observe that the vast majority of the trajectories obtained with the nonlinear model are bounded by that ones predicted with the two presented liner models.

C. Model discretization

Equations (7a), (7f), (9) and (10) describe linear continuous-time models. Their discretization is performed in two steps using a forward Euler approximation with a discretization time step Δt. Firstly, given the initial longitudinal position s_j and speed $\dot{x}_j$ at t_j and the braking or throttle effort $\bar{\beta}$, the longitudinal states can be computed over the prediction horizon H_p as

$$
\begin{aligned}
\dot{\bar{x}}_{k+1,j}^{\bar{\beta}} &= \dot{\bar{x}}_{k,j}^{\bar{\beta}} + \Delta t m_g \bar{\beta} - \Delta t k_d (\dot{\bar{x}}_{k,j}^{\bar{\beta}})^2 \\
\bar{s}_{k+1,j}^{\bar{\beta}} &= \bar{s}_{k,j}^{\bar{\beta}} + \Delta t \bar{x}_{k,j}^{\bar{\beta}} \\
\bar{t}_{k+1} &= \bar{t}_k + \Delta t
\end{aligned}
\tag{12}
$$

for $k = j, .., j+H_p-1$, where $\bar{s}_{j,j}^{\bar{\beta}} = s_j$, $\dot{\bar{x}}_{j,j}^{\bar{\beta}} = \dot{x}_j$ and $\bar{t}_j = t_j$. $\dot{\bar{x}}_{k,j}^{\bar{\beta}}$ and $\bar{s}_{k,j}^{\bar{\beta}}$ represent the longitudinal speed and position, respectively, at time $\bar{t}_k$, predicted at time t_j. Secondly, using the computed sequences $\tilde{s}_j^{\bar{\beta}} = \{\bar{s}_{j,j}^{\bar{\beta}}, .., \bar{s}_{j+H_p-1,j}^{\bar{\beta}}\}$ and $\dot{\tilde{x}}_j^{\bar{\beta}} = \{\dot{\bar{x}}_{j,j}^{\bar{\beta}}, .., \dot{\bar{x}}_{j+H_p-1,j}^{\bar{\beta}}\}$, and a suitable discretization scheme, the models (9) and (10) can be used to obtain LTV models of the lateral vehicle dynamics to be used in the MPC formulation. We denote the discretized conservative lateral dynamics model by

$$
\xi_{k+1,j}^{cm,\bar{\beta}} = A_{k,j}^{cm,\bar{\beta}} \xi_{k,j}^{cm,\bar{\beta}} + B_{k,j}^{cm,\bar{\beta}} u_{k,j}^{\bar{\beta}},
\tag{13}
$$

and the discretized overreacting lateral dynamics model by

$$
\xi_{k+1,j}^{om,\bar{\beta}} = A_{k,j}^{om,\bar{\beta}} \xi_{k,j}^{om,\bar{\beta}} + B_{k,j}^{om,\bar{\beta}} u_{k,j}^{\bar{\beta}},
\tag{14}
$$

for a given value of $\bar{\beta}$. The state vector of the models is defined as $\xi_{k,j}^{*,\bar{\beta}} = \{\dot{y}_{k,j}^{*,\bar{\beta}}, \dot{\psi}_{k,j}^{*,\bar{\beta}}, e_{\psi_{k,j}}^{*,\bar{\beta}}, e_{y_{k,j}}^{*,\bar{\beta}}, \delta_{k,j}^{*,\bar{\beta}}\}$, and the input is the steering rate $u_{k,j}^{\bar{\beta}}$.

III. Safety constraints

In this section, we show how the requirements of keeping the vehicle in the lane while avoiding obstacles and operating in a stable region can be expressed as constraints on the vehicle's states and input.

A. Actuator limits

The use of an Active Front Steering (AFS) unit to drive the steering angle imposes bound on the steering angle and its derivative. These bounds can be represented as linear constraints on the input and the state vector:

$$
-\delta_{lim} \leqslant \delta_{k,j}^{*,\bar{\beta}} \leqslant \delta_{lim}
\tag{15a}
$$

$$
-\dot{\delta}_{lim} \leqslant u_{k,j}^{\bar{\beta}} \leqslant \dot{\delta}_{lim},
\tag{15b}
$$

for $k = j, .., j+H_p-1$.

B. Slip angles bounds

The conservative and overreacting lateral dynamics model are valid for values of α_f and α_r satisfying (11). This requirement can be expressed as linear constraints on the state vector:

$$
\left| \frac{\dot{y}_{k,j}^{*,\bar{\beta}} + a\dot{\psi}_{k,j}^{*,\bar{\beta}}}{\bar{x}_{k,j}^{\bar{\beta}}} - \delta_{k,j}^{*,\bar{\beta}} \right| \leqslant \alpha_{f,lim}, \quad \left| \frac{\dot{y}_{k,j}^{*,\bar{\beta}} - b\dot{\psi}_{k,j}^{*,\bar{\beta}}}{\bar{x}_{k,j}^{\bar{\beta}}} \right| \leqslant \alpha_{r,lim},
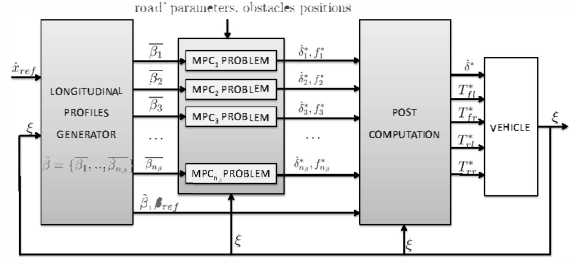\tag{16}
$$

for $k = j, .., j+H_p-1$.

Fig. 5.   Structure of the obstacle avoidance controller.

C. Lane boundaries

Lane boundaries can be easily introduced in the model as constraints on the lateral position error $e_{y_{k,j}}^{*,\bar{\beta}}$:

$$
|e_{y_{k,j}}^{*,\bar{\beta}}| \leqslant \frac{1}{2} l_w,
\tag{17}
$$

for $k = j, .., j + H_p - 1$, where l_w denotes the lane width.

D. Obstacle avoidance constraints

Finally, we show how static and moving obstacles can be expressed as additional linear constraints on the lateral position error $e_{y_{k,j}}^{*,\bar{\beta}}$. We introduce the following assumptions:

Assumption 6: The current and the future positions of all obstacles in the proximity of the vehicle are known as function of time.

Assumption 7: The controller knows the side of the obstacle on which it is safe to pass.

These assumptions allow us to map the obstacles' positions to a safe region on the road defined by its left and right bounds $e_{y,left}(t, s)$ and $e_{y,right}(t, s)$, respectively. Note that these bounds are a function of time t and position s along the road. The pre-computation of $\tilde{s}_j^{\bar{\beta}}$ defines a unique correspondence between $\bar{t}_j$ and $\bar{s}_{k,j}^{\bar{\beta}}$ (i.e. $\bar{s}_{k,j}(\bar{t}_k)$) for a given $\bar{\beta}$, and allows us to recast the obstacle avoidance problem as LTV constraints on the lateral position error:

$$
e_{y,right}(\bar{t}_k, \bar{s}_{k,j}(\bar{t}_k)) \leqslant e_{y_{k,j}}^{*,\bar{\beta}} \leqslant e_{y,left}(\bar{t}_k, \bar{s}_{k,j}(\bar{t}_k)), \tag{18}
$$

for $k = j, .., j + H_p - 1$.

E. Summary of constraints

The constraints (15a), (16), (17) and (18) can be compactly written as

$$
\xi_{k,j}^{*,\bar{\beta}_i} \in \Xi_{k,j}^{\bar{\beta}_i},
$$

for $k = j, .., j+H_p-1$, where $\Xi_{k,j}^{\bar{\beta}_i}$ is time-varying sequence of convex sets. The inequality (15b) can be rewritten as $u_{k,j}^{\bar{\beta}_i} \in \mathcal{U}$ for $k = j, .., j + H_p - 1$, where the set $\mathcal{U}$ is convex.

IV. Controller design

In this section we describe the MPC architecture used to address the obstacle avoidance problem. As shown in Figure 5, we decompose the controller into three sequential blocks: longitudinal profiles generation (A), MPC problems (B) and post-computation (C).

A. Longitudinal profiles generation

The *longitudinal profiles generator* block is responsible for defining a set of n_β possible braking ratio commands $\bar{\beta} = \{\bar{\beta}_1, .., \bar{\beta}_{n_\beta}\}$ and a reference braking ratio β_{ref} computed using a PI controller which tracks a given reference speed v_{ref}. In our work, we have investigated two different definitions of the set of braking ratios:

- n_β *braking ratios*: In this approach, we consider the braking ratios to be n_β uniformly spaced points in the interval $[\bar{\beta}_1, \bar{\beta}_{n_\beta}]$. While $\bar{\beta}_1$ is set to -1, $\bar{\beta}_{n_\beta}$ depends on the sign of β_{ref}: if $\beta_{ref} \leqslant 0$, then $\bar{\beta}_{n_\beta} = 0$; otherwise $\bar{\beta}_{n_\beta} = \beta_{ref}$.
- 3 *braking ratios*. This definition of the braking ratios set $\bar{\beta} = \{\bar{\beta}_1, \bar{\beta}_2, \bar{\beta}_{n_\beta}\}$ is a consequence of the observation that the optimal braking ratio β^* changes slowly with time. Hence, given the last two optimal braking ratios β_p^* and β_{pp}^*, $\bar{\beta}$ is computed as follows:

$$\bar{\beta} = \begin{cases} \{\beta_p^* - \Delta\beta, \beta_p^*, \beta_p^* + \Delta\beta\} & \text{if} \quad \beta_p^* = \beta_{pp}^* \\ \{\beta_p^*, \beta_p^* + \Delta\beta, \beta_p^* + 2\Delta\beta\} & \text{if} \quad \beta_p^* > \beta_{pp}^* \\ \{\beta_p^* - 2\Delta\beta, \beta_p^* - \Delta\beta, \beta_p^*\} & \text{if} \quad \beta_p^* < \beta_{pp}^*, \end{cases}$$

where the perturbation $\Delta\beta$ is a parameter to be chosen.

B. MPC problems

This block formulates and solves the constrained finite time optimal control problem at each time step. Using (12) for every $\bar{\beta}_i$, $i = 1, .., n_\beta$, the sequence of longitudinal positions $\tilde{s}_j^{\bar{\beta}_i}$ and speeds $\tilde{\dot{x}}_j^{\bar{\beta}_i}$ over the prediction horizon H_p is computed. The MPC formulation predicts the vehicle's states using both the *conservative lateral dynamic model* and the *overreacting lateral dynamic model*. The states predicted over the horizon H_p using *conservative lateral dynamic model* play the main role and they appear both in the cost function and in the constraints. The *overreacting lateral dynamic model*, instead, has an auxiliary role and it is used with a shorter prediction horizon H_{p2} in the constraints definition. The MPC problem can be synthesized as follows:

$$\min_{U_j^{\bar{\beta}_i}} \quad J_N(\tilde{\xi}_j^{cm,\bar{\beta}_i}, U_j^{\bar{\beta}_i}) \tag{19a}$$

$$\text{subj. to} \quad \xi_{k+1,j}^{cm,\bar{\beta}_i} = A_k^{cm,\bar{\beta}_i} \xi_{k,j}^{cm,\bar{\beta}_i} + B_k^{cm,\bar{\beta}_i} u_{k,j}^{\bar{\beta}_i}, \tag{19b}$$
$$k = j, .., j + H_p - 1$$

$$\xi_{k+1,j}^{om,\bar{\beta}_i} = A_k^{om,\bar{\beta}_i} \xi_{k,j}^{om,\bar{\beta}_i} + B_k^{om,\bar{\beta}_i} u_{k,\bar{\beta}_i}, \tag{19c}$$
$$k = j, .., j + H_{p2} - 1$$

$$u_{k,j}^{\bar{\beta}_i} \in \mathcal{U} \qquad k = j, .., j + H_p - 1 \tag{19d}$$

$$\xi_{k,j}^{cm,\bar{\beta}_i} \in \Xi_{k,j}^{\bar{\beta}_i} \quad k = j, .., j + H_p - 1 \tag{19e}$$

$$\xi_{k,j}^{om,\bar{\beta}_i} \in \Xi_{k,j}^{\bar{\beta}_i} \quad k = j, .., j + H_{p2} - 1 \tag{19f}$$

$$\xi_{j,j}^{cm,\bar{\beta}_i} = \xi_{j,j}^{om,\bar{\beta}_i} = \xi(t_j), \tag{19g}$$

where $J_N(\tilde{\xi}_j^{cm,\bar{\beta}_i}, U_j^{\bar{\beta}_i})$ is a convex quadratic function depending on the states, the slip angles and the input. $\tilde{\xi}_j^{cm,\bar{\beta}_i} = \{\xi_{j,j}^{cm,\bar{\beta}_i}, \xi_{j+1,j}^{cm,\bar{\beta}_i}, ..., \xi_{j+H_p-1,j}^{cm,\bar{\beta}_i}\}$ is the sequence of states over the prediction horizon H_p predicted at time t_j, and updated according to the discretized *conservative lateral dynamics model* (13). $\tilde{\xi}_j^{om,\bar{\beta}_i} = \{\xi_{j,j}^{om,\bar{\beta}_i}, \xi_{j+1,j}^{om,\bar{\beta}_i}, ..., \xi_{j+H_{p2}-1,j}^{cm,\bar{\beta}_i}\}$ is the sequence of states

over the prediction horizon H_{p2} predicted at time t_j, and updated according to the discretized *overreacting lateral dynamics model* (14). $u_{k,j}^{\bar{\beta}_i} \in \mathbb{R}^{m_r}$ is the kth vector of the input sequence $U_j^{\bar{\beta}_i} = \{u_{j,j}^{\bar{\beta}_i}, ..., u_{j+H_p-1,j}^{\bar{\beta}_i}\}^T \in \mathbb{R}^{m_r H_p}$. Since the models and the constraints are linear, it is possible to formulate every MPC problem as a QP. Each MPC controller in Figure 5 returns the optimal steering rate u_i^* and the optimal value of the cost function $f_{i,lat}^*$. In order to reduce the computational complexity, the input is kept constant for every H_i time-steps (i.e. $u_{j+iH_i+k,j}^{\bar{\beta}_i} = u_{j+iH_i,j}^{\bar{\beta}_i}$ for $k = 1, ..., H_i - 1$, $i = 0, ..., (H_p/H_i)$). With this simplification the number of optimization variables can be significantly reduced, speeding up the computations.

C. Post-computation

In the *post-computation* block, the optimal cost functions $f_{i,lat}^*$ are augmented by adding a quadratic term representing the deviation of $\bar{\beta}_i$ from β_{ref} as follows,

$$f_i^* = f_{i,lat}^* + ||\bar{\beta}_i - \beta_{ref}||_{Q_\beta}^2,$$

The optimal braking ratio β^* and the corresponding steering rate $\dot{\delta}^*$ can be then computed as,

$$(\beta^*, \dot{\delta}^*) = \{(\beta_i^*, \dot{\delta}_i^*) : f_i^* = \min(f_1^*, .., f_{n_\beta}^*)\}.$$

V. SIMULATION AND EXPERIMENTAL RESULTS

In this section we present the obtained results through simulations and real experiments.

A. Simulation setup description and results

Hardware-in-the-loop simulations of the controller are performed on a dSPACE rapid prototyping system consisting of a DS1401 MicroAutoBox (IBM PowerPC 750FX processor, 800 MHz) and a DS1006 processor board (Quad-core AMD Opteron processor, 2.8 GHz). The controller runs on the MicroAutoBox, and the DS1006 board simulates the vehicle dynamics using a nonlinear four wheel vehicle model with a Pacejka tire model.

The simulations have been performed using the following parameters: $H_p = 45$, $H_{p2} = 20$ and $H_i = 3$. The considered scenarios consist of a straight slippery road ($\mu = 0.3$) with one or more static obstacles. The edge of each obstacle is at a distance of 2 m from the road centerline. Note that no tolerance has been added to the lane or obstacle bounds to account for the vehicle's width.

Figure 6 shows the path of the vehicle while avoiding a single obstacle, while Figure 7 shows the path of the vehicle while avoiding two obstacles. The vehicle is able to avoid the obstacles and return to the lane centerline in both cases. Moreover, the vehicle travels close to the obstacle while avoiding it.

B. Experimental setup description

The experiments were performed on a Jaguar S–type vehicle ($m = 2050$ kg, $I = 3344$ kg-m^2) at the Smithers winter testing center (Raco, MI, U.S.A.) on tracks covered with packed snow ($\mu \approx 0.3$). A picture of the vehicle and the environment is shown in Figure 8. The vehicle is equipped with an Active Front Steering (AFS) system and four wheel independent braking. An Oxford Technical Solutions (OTS) RT3002 sensing system is used to measure the position and orientation in the inertial frame, and the vehicle velocities in the body frame. The OTS RT3002 system comprises
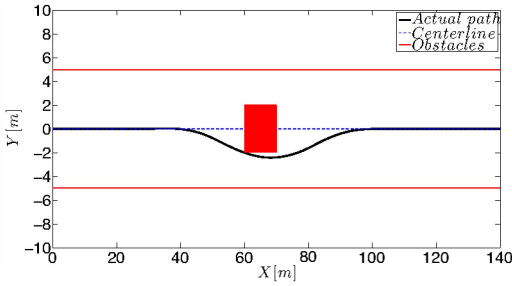
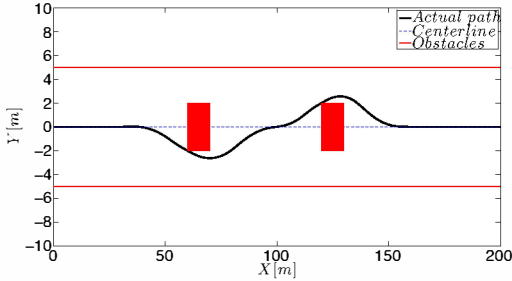Fig. 6. **Simulation 1:** The vehicle avoids one obstacle with an entry speed of 50 kph.

Fig. 7. **Simulation 2:** The vehicle avoids two obstacles with an entry speed of 50 kph.

of a differential GPS, an IMU and a DSP. The real-time computations are performed on a dSPACE DS1005 Autobox system which consists of a PowerPC 750GX processor running at 933 MHz.

The simulations have been performed using the following parameters: $H_p = 30$, $H_{p2} = 20$ and $H_i = 3$.

The test scenario consists of a straight road with a single obstacle. The edge of the obstacle is a distance of 1.5 m from the road centerline. The path of the vehicle is shown in Figure 9. It is seen that the vehicle avoids the obstacle and returns to the road centerline with a low overshoot. The performance is similar to that seen in simulations. Note that the scenario with two obstacles was not considered in the experiments due to the lack of testing time.

VI. CONCLUSIONS

We have presented a LTV model of the vehicle dynamics, and used it to formulate an MPC problem for obstacle avoidance and lane keeping. The linearity of the model and convexity of the constraints is used to recast the MPC problem as a set of QP subproblems. The low computational complexity of each subproblem allows us to solve the MPC

Fig. 8. Experimental setup: Jaguar S-Type test vehicle driving on snow
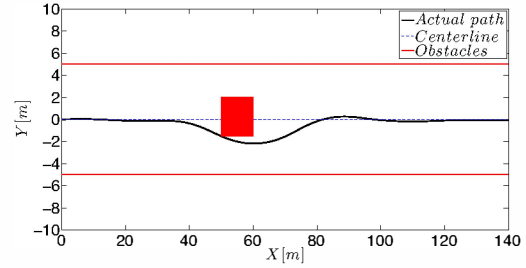

Fig. 9. **Experimental result:** The vehicle is able to avoid the obstacle with an entry speed of 50 kph.

problem in real-time while using long prediction horizons. Future work involves exploring customized embedded QP solvers for the fast solution of each QP.

VII. ACKNOWLEDGMENTS

REFERENCES

[1] R. Subramanian, "Motor vehicle traffic crashes as a leading cause of death in the united states, 2008 and 2009," *U.S. Department of Trasportation*, 2012.

[2] M. Bertozzi, A. Broggi, and A. Fascioli, "Vision-based intelligent vehicles: State of the art and perspectives," *Robotics and Autonomous Systems*.

[3] M. Pollefeys, D. Nistr, J.-M. Frahm, A. Akbarzadeh, P. Mordohai, B. Clipp, C. Engels, D. Gallup, S.-J. Kim, P. Merrell, C. Salmi, S. Sinha, B. Talton, L. Wang, Q. Yang, H. Stewnius, R. Yang, G. Welch, and H. Towles, "Detailed real-time urban 3D reconstruction from video," *International Journal of Computer Vision*, vol. 78, pp. 143–167, 2008. [Online]. Available: http://dx.doi.org/10.1007/s11263-007-0086-4

[4] F. Ferrari, E. Grosso, G. Sandini, and M. Magrassi, "A stereo vision system for real time obstacle avoidance in unknown environment," in *Intelligent Robots and Systems '90. 'Towards a New Frontier of Applications', Proceedings. IROS '90. IEEE International Workshop on*, 1990.

[5] S. J. Anderson, S. C. Peters, T. E. Pilutti, and K. Iagnemma, "An optimal-control-based framework for trajectory planning, threat assessment, and semi-autonomous control of passenger vehicles in hazard avoidance scenarios," *International Journal of Vehicle Autonomous Systems*, vol. 8, no. 2, pp. 190–216, 2010.

[6] P. Falcone, F. Borrelli, J. Asgari, H. E. Tseng, and D. Hrovat, "Predictive active steering control for autonomous vehicle systems," *IEEE Trans. on Control System Technology*, vol. 15, no. 3, 2007.

[7] P. Falcone, B. Borrelli, J. Asgari, H. E. Tseng, and D. Hrovat, "Low complexity MPC schemes for integrated vehicle dynamics control problems," 9th *International Symposium on Advanced Vehicle Control*, 2008.

[8] Y. Gao, T. Lin, F. Borrelli, E. Tseng, and D. Hrovat, "Predictive control of autonomous ground vehicles with obstacle avoidance on slippery roads," *Dynamic Systems and Control Conference, 2010*, 2010.

[9] Y. Gao, A. Gray, J. Frasch, T. Lin, E. Tseng, J. Hedrick, and F. Borrelli, "Spatial predictive control for agile semi-autonomous ground vehicles," 13th *International Symposium on Advanced Vehicle Control*, 2012.

[10] A. Gray, M. Ali, Y. Gao, J. Hedrick, and F. Borrelli, "Integrated threat assessment and control design for roadway departure avoidance," in *Intelligent Transportation Systems (ITSC), 2012 15th International IEEE Conference on*, Sept., pp. 1714–1719.

[11] D. Margolis and J. Asgari, *Multipurpose Models of Vehicle Dynamics for Controller Design*. Society of Automotive Engineers, 1991.

[12] H. Pacejka, *Tire and Vehicle Dynamics*. Elsevier Science, 2012. [Online]. Available: http://books.google.se/books?id=926T_pblHqQC